This paper is published as part of a *Dalton Transactions* themed issue entitled:

New Talent: Americas

Guest Editors: John Arnold, Dan Mindiola, Theo Agapie, Jennifer Love and Mircea Dincă

Published in issue 26, 2012 of *Dalton Transactions*

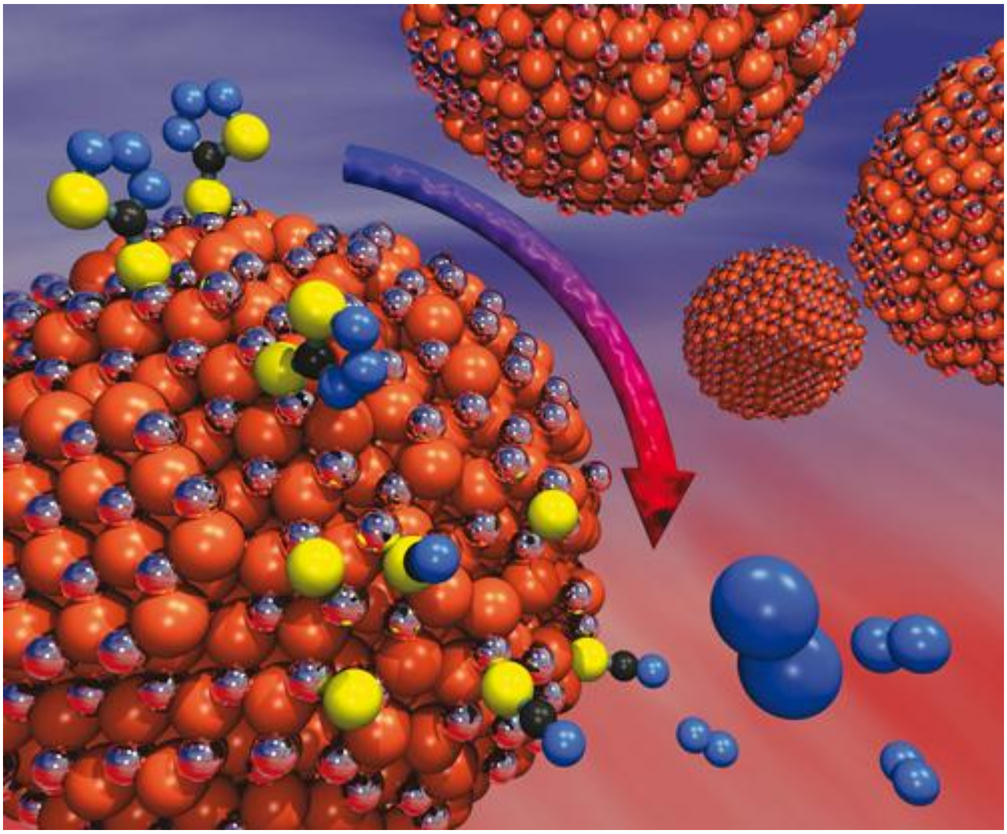

Image reproduced with permission of Richard L. Brutchey

Articles published in this issue include:

Dalton Transactions

Dynamic Article Links

Cite this: *Dalton Trans.*, 2012, **41**, 7931

www.rsc.org/dalton

PAPER

Investigation of the synthesis, activation, and isosteric heats of CO_2 adsorption of the isostructural series of metal–organic frameworks $M_3(BTC)_2$ (M = Cr, Fe, Ni, Cu, Mo, Ru)†

Casey R. Wade and Mircea Dincă*

Received 16th February 2012, Accepted 26th March 2012
DOI: 10.1039/c2dt30372h

The synthesis, activation, and heats of CO_2 adsorption for the known members of the $M_3(BTC)_2$ (HKUST-1) isostructural series (M = Cr, Fe, Ni, Zn, Ni, Cu, Mo) were investigated to gain insight into the impact of CO_2–metal interactions for CO_2 storage/separation applications. With the use of modified syntheses and activation procedures, improved BET surface areas were obtained for M = Ni, Mo, and Ru. The zero-coverage isosteric heats of CO_2 adsorption were measured for the Cu, Cr, Ni, Mo, and Ru analogues and gave values consistent with those reported for MOFs containing coordinatively unsaturated metal sites, but lower than for amine functionalized materials. Notably, the Ni and Ru congeners exhibited the highest CO_2 affinities in the studied series. These behaviors were attributed to the presence of residual guest molecules in the case of $Ni_3(BTC)_2(Me_2NH)_2(H_2O)$ and the increased charge of the dimetal secondary building unit in $[Ru_3(BTC)_2][BTC]_{0.5}$.

Introduction

Owing to their microporous structures and high surface areas, metal–organic frameworks (MOFs) continue to receive significant attention as materials with potential for applications in gas storage and separation.[1–8] Within this scope, more recent efforts have been devoted to developing these materials for the capture and separation of CO_2.[7,9–14] Two common strategies for enhancing the CO_2 affinity and selectivity in MOFs include functionalization of the frameworks with amines or other basic groups,[15–23] and removal of terminal bound solvent molecules to expose coordinatively-unsaturated metal centers (UMCs).[24–39] The former relies on chemisorptive interactions inspired by liquid amine scrubbers,[40,41] while the benefit of the latter is commonly ascribed to a physisorptive process enhanced by ion-induced dipole interactions.[42] Although the UMC approach has been exploited extensively in structurally unrelated materials, few studies exist wherein an *isostructural* MOF series has been explored to determine trends among various metal ions.[42–45] Such studies are valuable because they can eliminate all other variables that may influence CO_2 uptake such as pore size, pore shape and apparent surface area, thereby providing direct insight into the nature of the CO_2–metal interaction. One notable example is the family of materials known as MOF-74: M_2(DOBDC) (M = Mg, Co, Ni; DOBDC = 2,5-dioxy-1,4-benzenedicarboxylate). In this series, X-ray and neutron diffraction experiments have shown that UMCs are the initial sites of interaction of CO_2 with the framework in Mg_2(DOBDC)[42,46] and Ni_2(DOBDC),[29] while CO_2 adsorption isotherms measured at various temperatures revealed that the strength of initial interaction varies as Mg > Ni > Co.[28] Studies determined across isostructural series therefore provide important insight into the relative strength of the guest–framework interactions, which are a key to the efficient capture and release of CO_2.

Despite the vast number of MOFs synthesized, relatively few can be placed into an isostructural series, and even fewer can conceivably support UMCs. However, one of the earliest MOFs in which the presence of UMCs was evidenced, $Cu_3(BTC)_2$ (BTC = 1,3,5-benzentricarboxylate),[47] has become one of the most emblematic and is part of an isostructural series that currently includes Cr, Fe, Ni, Zn, Mo, and Ru analogues. The structure of $Cu_3(BTC)_2$, shown in Fig. 1, contains dicopper paddlewheel secondary building units (SBUs) bridged by four carboxylate groups. The solvent molecules which occupy the axial sites on each Cu^{2+} ion can be readily removed by heating under vacuum to generate UMCs. Despite the popularity of $Cu_3(BTC)_2$ in a range of applications, including CO_2 storage, its analogues have received much less attention and none have been tested for CO_2 uptake. For instance, $Cr_3(BTC)_2$[48] and $Mo_3(BTC)_2$,[49] containing quadruply bonded dimetal units, were shown to exhibit permanent porosity and high surface areas comparable to $Cu_3(BTC)_2$, but gas sorption studies were limited to H_2, N_2, and O_2. The other known analogs include $Zn_3(BTC)_2$,[50,51] $Ni_3(BTC)_2$,[52] and the mixed-valent Fe(II/III) and Ru(II/III) structures $Fe_3(BTC)_2Cl$[53] and $Ru_3(BTC)_2(Cl)_x(OH)_{1.5-x}$.[54] Although $Ni_3(BTC)_2$ and $Ru_3(BTC)_2(Cl)_x(OH)_{1.5-x}$ were shown

Department of Chemistry, Massachusetts Institute of Technology, 77 Massachusetts Avenue, Cambridge, Massachusetts 02139, United States. E-mail: mdinca@mit.edu

† Electronic supplementary information (ESI) available: Additional spectral data. See DOI: 10.1039/c2dt30372h

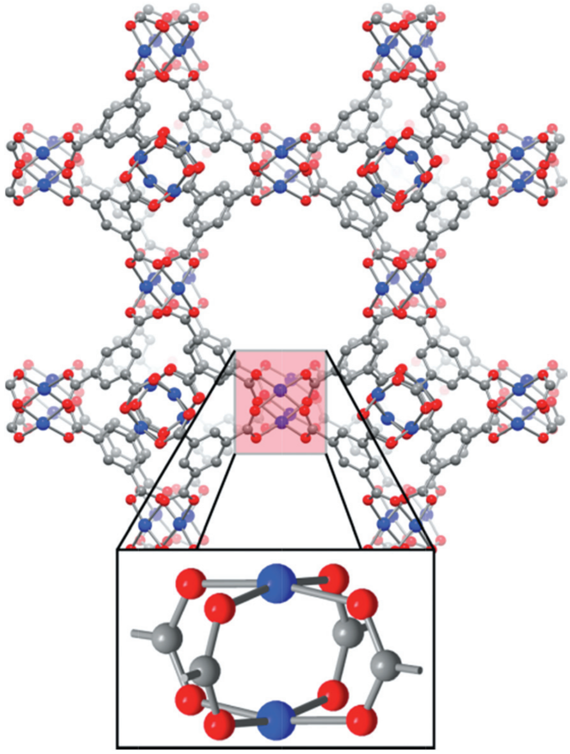

Fig. 1 Portion of the crystal structure of $M_3(BTC)_2$, highlighting the dimetallic tetracarboxylate SBU. Blue, red, and grey spheres represent metal, O, and C atoms, respectively. H atoms and axial ligands on the SBU were omitted for clarity.

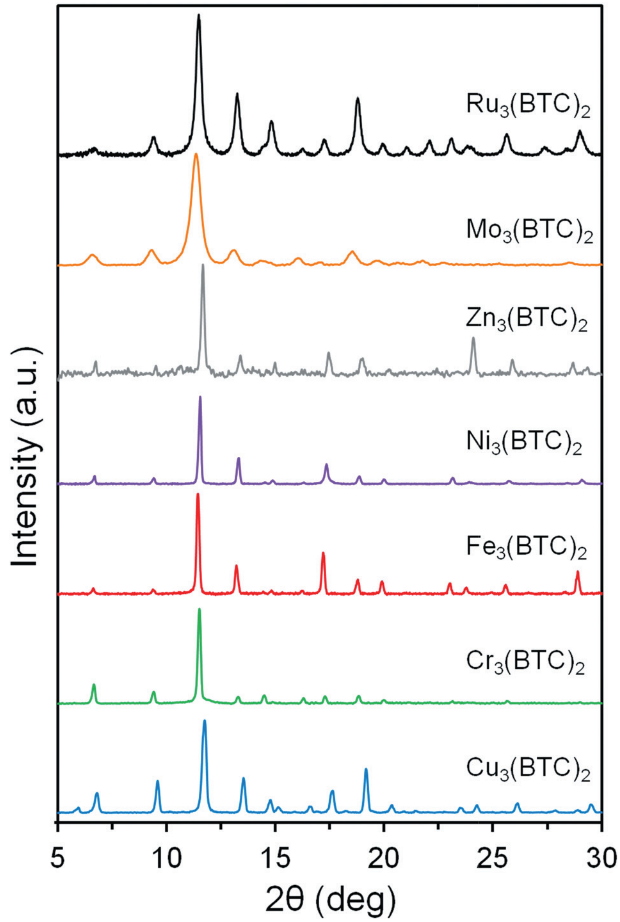

Fig. 2 Experimental powder X-ray diffraction patterns showing the isostructural relationship among the $M_3(BTC)_2$ series (M = Cu, Cr, Fe, Ni, Zn, Mo, Ru).

to exhibit permanent porosity, their reported BET surface areas were lower than those obtained for $Cu_3(BTC)_2$, despite the isostructural relationship, and no associated CO_2 sorption data was reported. In an effort to gain insight into the value of CO_2–UMC interactions for CO_2 storage/separation applications, we examined the synthesis, activation, and CO_2 uptake properties of the reported members of the $M_3(BTC)_2$ isostructural series.

Table 1 Apparent BET surface areas and isosteric heats of CO_2 adsorption measured for the porous members of the $M_3(BTC)_2$ series

	BET SA/m^2 g^{-1}	BET SA/m^2 $mmol^{-1}$	$-\Delta H_{ads}(CO_2)$/ kJ mol^{-1}
$Cu_3(BTC)_2$	1734 ± 1 (2153)[a]	1049 ± 1 (1301)[a]	29.8 ± 0.2
$Cr_3(BTC)_2$	2031 ± 6	1158 ± 2	26.7 ± 0.2
$Ni_3(BTC)_2(Me_2NH)_2(H_2O)$	1047 ± 1	732 ± 1	36.8 ± 0.4
$Mo_3(BTC)_2(DMF)_{0.5}$	1689 ± 5	1264 ± 3	25.6 ± 0.6
$[Ru_3(BTC)_2][BTC]_{0.5}$	1180 ± 5	969 ± 4	32.6 ± 0.4

[a] Calculated geometric accessible surface area from ref. 60.

Results and discussion

$Cu_3(BTC)_2$ and $Cr_3(BTC)_2$ are both known to have fully activated SBUs, permanent porosity, and measured surface areas consistent with those predicted from the crystal structures. Accordingly, they were prepared and activated as previously described, and their powder X-ray diffraction patterns matched those expected (Fig. 2).[48,55] The BET surface area of 1734(±1) m^2 g^{-1} measured by us for $Cu_3(BTC)_2$ falls near the upper end of the reported values for this material, which range from 692–1944 m^2 g^{-1},[56–59] and is in line with the geometric accessible surface area previously calculated from the crystal structure (2153 m^2 g^{-1})[60] (Table 1, Fig. 3). Likewise, an N_2 adsorption isotherm measured for $Cr_3(BTC)_2$ afforded a BET surface area of 2031(±6) m^2 g^{-1}, higher than the previously reported value of 1810 m^2 g^{-1}.[48]

Although the synthesis of $Ni_3(BTC)_2$ was recently reported, the authors noted a difficulty in scaling-up the high-throughput screening conditions. We attempted to repeat this procedure on a larger scale (0.5–1.0 g) using both glass and Teflon-lined reactors and obtained mixtures of dark green crystals and brown powders in both cases. The green crystals could be mechanically separated from the brown powders by washing and decanting from *N*,*N*′-dimethylformamide (DMF) and gave powder X-ray diffraction patterns consistent with the $M_3(BTC)_2$ structure type (Fig. 2). Thermogravimetric analysis (TGA) of the sample showed a gradual desorption of solvent over the 25–200 °C range, followed by the onset of rapid mass loss after 250 °C (Fig. S1†). In accordance with the TGA and the previously described procedure, $Ni_3(BTC)_2$ was activated by heating under vacuum at 150 °C for 12 h. After this activation procedure, the

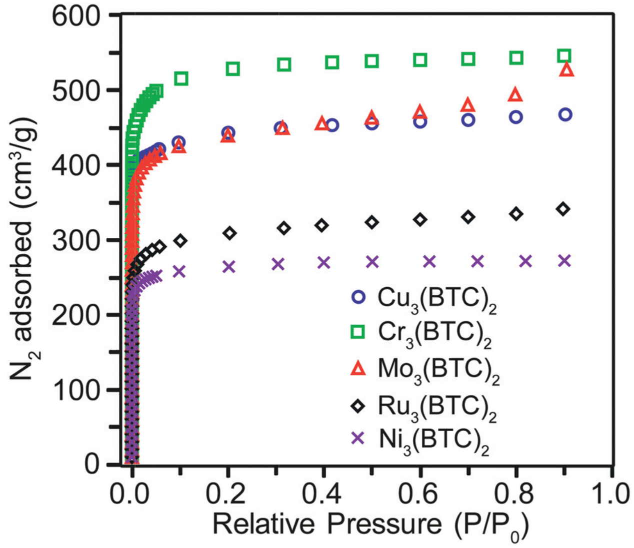

Fig. 3 Isotherms for the adsorption of N_2 in $M_3(BTC)_2$ (M = Cu, Cr, Mo, Ru, Ni) at 77 K.

material exhibited a BET surface area of 847(±3) $m^2\ g^{-1}$, only slightly lower than the reported value of 920 $m^2\ g^{-1}$. In the initial report, single crystal X-ray diffraction and elemental analysis supported an empirical formula of $Ni_3(BTC)_2(Me_2NH)_3(DMF)_4(H_2O)_4$ in which DMF and H_2O guest molecules occupied the pores, while dimethylamine molecules produced by the *in situ* decomposition of DMF were bound to the axial positions of the Ni^{2+} centers. The lower surface area in comparison to $Cu_3(BTC)_2$ was attributed to incomplete evacuation of the guest molecules. In an effort to improve the activation procedure and achieve a higher surface area, we carried out a solvent exchange by soaking a sample of the as-synthesized $Ni_3(BTC)_2$ in anhydrous methanol for 24 h. This approach of exchanging DMF and other high boiling solvents with more volatile ones has proven effective at facilitating evacuation and exposing UMCs in other MOFs.[61] After this treatment, powder X-ray diffraction confirmed retention of sample crystallinity, and FT-IR spectroscopy showed the disappearance of the DMF ν(C═O) stretching band at 1670 cm^{-1} (Fig. S2†).

The TGA profile for the methanol exchanged sample displayed a ~11% weight loss up to 150 °C, which was attributed to the desorption of methanol solvent, and a rapid mass loss around 300 °C that likely corresponds to framework decomposition (Fig. S3†). The sample was subsequently activated at 150 °C for 12 h. Although this treatment did not affect bulk crystallinity (Fig. S4†), the apparent BET surface area of this material was 1047(±1) $m^2\ g^{-1}$, still somewhat low in comparison to $Cu_3(BTC)_2$ and $Cr_3(BTC)_2$. Elemental analysis (C, H, N) of the activated sample matched the formula $Ni_3(BTC)_2(Me_2NH)_2(H_2O)$, suggesting that guest molecules are instead responsible for the decreased surface area. While no clear O–H stretching (3000–3600 cm^{-1}) band is observed in the FT-IR spectrum of $Ni_3(BTC)_2(Me_2NH)_2(H_2O)$ under N_2, the H–O–H bending mode in the 1600 cm^{-1} region supports the presence of residual H_2O while the aliphatic C–H stretches below 3000 cm^{-1} and weak N–H stretch at 3260 cm^{-1} indicate the presence of residual Me_2NH in the activated sample (Fig. S5†).[62–65]

Dark orange-red crystals of $Fe_3(BTC)_2Cl$ could easily be obtained according to the reported procedure by heating a mixture of $FeCl_3$, 1,4-diazabicyclo-[2.2.2]-octane (DABCO), and H_3BTC in DMF in a sealed Teflon bomb at 150 °C.

However, in line with the previous report, samples obtained under these conditions exhibited no measurable porosity after attempted activation procedures which included solvent exchange with MeOH or CH_2Cl_2 followed by heating in vacuum or supercritical CO_2 drying. Upon heating a sample of as-synthesized $Fe_3(BTC)_2Cl$ under vacuum during attempted activation, a small amount of white residue was observed to sublime from the sample. ^{1}H NMR analysis of this residue showed a singlet resonance at 2.70 ppm, indicative of DABCO (Fig. S6†). Speculating that DABCO may block the Fe sites and/or the pores in these samples, we sought alternative pathways to access guest-free $Fe_3(BTC)_2$. Nevertheless, alternative synthetic procedures excluding the use of DABCO or starting from $FeCl_2$ failed to consistently give phase-pure material.

We completed our survey of the $M_3(BTC)_2$ series containing first row transition metals by examining the synthesis and activation of $Zn_3(BTC)_2$. Matzger and coworkers have recently reported the failure of $Zn_3(BTC)_2$ to display permanent accessible porosity.[51] Based on positron annihilation lifetime spectroscopy experiments, they suggested that although the framework retains crystallinity and bulk porosity, surface collapse upon drying effectively blocks guest access to the framework pores. We repeated their reported synthesis of $Zn_3(BTC)_2$ and found that the material indeed shows no measurable N_2 uptake upon activation by heating in vacuum. Consequently, we turned our attention to the synthesis and activation of members of the $M_3(BTC)_2$ series containing the second row transition metals Mo and Ru.

$Mo_3(BTC)_2$ was isolated as an air-sensitive orange–red powder by heating a mixture of $Mo(CO)_6$ and H_3BTC at reflux in DMF according to a literature procedure.[49] The crystallinity of this product and its isostructural relationship to $Cu_3(BTC)_2$ were confirmed by powder X-ray diffraction (Fig. 2). Notably, the reported activation procedure leaves a significant amount of DMF in the material (~1 DMF per Mo), which presumably binds to the Mo centers leaving few, if any, unsaturated metal sites. To minimize the amount of DMF retained in $Mo_3(BTC)_2$, the as-synthesized material was exchanged by soaking a sample in anhydrous methanol for 1 week and refreshing the methanol solution daily. TGA analysis of the methanol exchanged sample showed a 12% weight loss in the 25–150 °C range, which corresponds to the loss of ~3 molecules of methanol (Fig. S7†). Gratifyingly, a sample of methanol-exchanged $Mo_3(BTC)_2$ heated under vacuum at 100 °C for 12 h and at 150 °C for 24 h provided a material with an apparent BET surface area of 1689 (±5) $m^2\ g^{-1}$, considerably higher than the previously reported value (1280 $m^2\ g^{-1}$). Elemental analysis (C, H, N) of the activated sample matched an empirical formula of $Mo_3(BTC)_2(DMF)_{0.5}$, indicating that only a small amount of DMF molecules remain trapped in the pores and a significant number of metal sites should be exposed. In fact, the remaining DMF could not be clearly assigned in the FT-IR spectrum of the sample (Fig. 4). However, the symmetric ν(Mo–Mo) stretching mode is readily observable by Raman spectroscopy, and an observed shift of this band to higher energy was previously proposed to

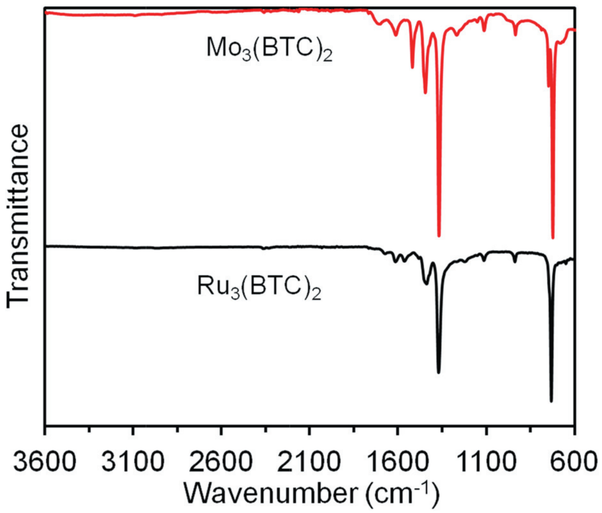

Fig. 4 FT-IR spectra of evacuated samples of $Mo_3(BTC)_2(DMF)_{0.5}$ and $[Ru_3(BTC)_2][BTC]_{0.5}$.

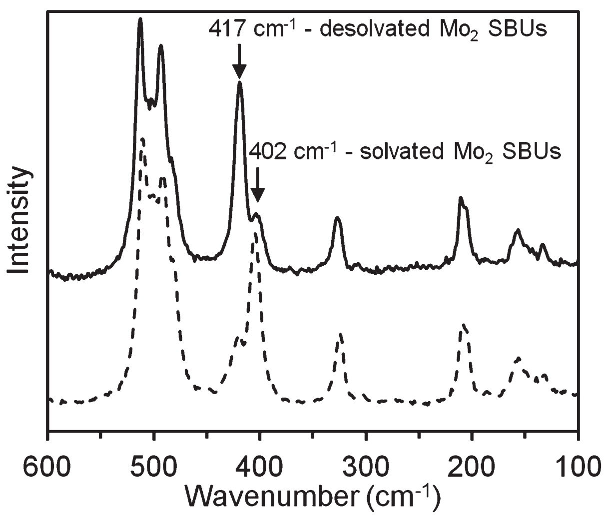

Fig. 5 Raman spectra of $Mo_3(BTC)_2$ recorded after solvent exchange with methanol (- - -) and after activation of the methanol-exchanged sample by heating under vacuum (—).

indicate desolvation of the Mo_2 SBUs in $Mo_3(BTC)_2$. The Raman spectrum of our methanol-exchanged sample of $Mo_3(BTC)_2$ shows two distinct ν(Mo–Mo) bands: an intense signal at 402 cm^{-1} and weaker one at 417 cm^{-1} (Fig. 5). These indicate that the methanol exchange procedure followed by brief drying under vacuum at room temperature initially activates a small number of the Mo_2 SBUs. After heating in vacuum, the increase in intensity of the band at 417 cm^{-1} indicates further activation of the material and the generation of a greater number of UMCs. The remaining shoulder at 402 cm^{-1} in the evacuated sample agrees with the presence of a small number of coordinated DMF molecules in the structure.

Our attempts to synthesize $Ru_3(BTC)_2$ starting from $RuCl_3{\cdot}xH_2O$ or $Ru_2Cl(\mu\text{-OAc})_4$ according to literature procedures yielded either amorphous products or poorly crystalline materials.[54] Increasing the reaction temperature above that reported in the literature (160 °C) produced significant amounts of Ru metal. However, employing $Ru_2Cl(\mu\text{-OPiv})_4$ (OPiv = $^{-}O_2C\text{–}C(CH_3)_3$) as the ruthenium source under the reported reaction conditions afforded material with a higher degree of crystallinity (Fig. S8†). TGA analysis showed steady weight loss from room temperature to around 300 °C (Fig. S9†), prompting us to attempt activation of the as-synthesized $Ru_3(BTC)_2$ by heating at 150 °C under vacuum for 48 h. An N_2 adsorption isotherm on the activated material revealed an apparent BET surface area of 1180(±5) m^2 g^{-1}, significantly higher than that measured in the earlier report (704 m^2 g^{-1}). Although the reported material has been formulated as $Ru_3(BTC)_2(Cl)_x(OH)_{1.5-x}$, elemental analysis of our activated sample showed only trace amounts of chlorine, suggesting that Cl^- does not provide the charge balance for the $\{Ru_2\}^{5+}$ paddlewheel units. While pivalate or acetate counteranions cannot be ruled out, their presence is unlikely based on the absence of aliphatic C–H stretching bands in the 2800–3000 cm^{-1} region of the IR spectrum of the activated sample (Fig. 4). In fact, elemental analysis (C, H) of the activated sample matches well with the charge balanced formula $[Ru_3(BTC)_2][BTC]_{0.5}$, which suggests that BTC^{3-} anions residing in the pores provide charge balance for the $\{Ru_2\}^{5+}$ units and are likely responsible for the slightly decreased BET surface area *versus* the Cu, Cr, and Mo congeners.

While the measured BET surface areas of $Cu_3(BTC)_2$ and $Cr_3(BTC)_2$ compare well with the literature values,[48,56–59] the synthetic and activation protocols adopted for $Ni_3(BTC)_2$, $Mo_3(BTC)_2$, and $Ru_3(BTC)_2$ resulted in higher BET surface areas than those previously reported. A better comparison of these values is provided by expressing them in m^2 mmol^{-1} of $M_3(BTC)_2(\text{guest})_x$ to account for the greater bulk density of $Mo_3(BTC)_2$ and $Ru_3(BTC)_2$ and the presence of guest molecules. As shown in Table 1, the values of the surface areas expressed in these units are similar for the Cu, Cr, and Mo analogs, while that of $[Ru_3(BTC)_2][BTC]_{0.5}$ shows it is slightly less porous, as expected based on the presence of guest BTC^{3-} anions. The apparent molar surface area of 716 m^2 mmol^{-1} for $Ni_3(BTC)_2(Me_2NH)_2(H_2O)$ activated after methanol exchange is appreciably lower than the other members of the series, presumably due to the $MeNH_2$ and H_2O guest molecules. Given the high surface areas exhibited by the Cu, Cr, Mo, and Ru samples, it is reasonable to assume that UMCs are being generated during the activation procedures, and therefore we set out to probe the effects of the identity of these open metal sites on CO_2 affinity.

CO_2 adsorption isotherms were measured for the activated MOFs from 0–800 Torr at three temperatures over the 313–334 K range. The isotherms, shown in Fig. 6, were fitted to virial equations similar to those previously used to describe gas–solid adsorption.[66] The isosteric heats of adsorption were then calculated using the virial coefficients from the fitting procedure and a modified Clausius–Clapeyron equation.[61]

Even at the lowest measurement temperature, the maximum CO_2 loading did not exceed 0.7 molecules of CO_2 per metal at 800 Torr for any of the studied MOFs, ensuring that the enthalpy values are representative of the interaction between CO_2 molecules with the strongest binding sites in each material. However, at these measurement temperatures (313–334 K), the adsorbed CO_2 molecules should be expected to sample a number of strong binding sites, both at the UMCs and framework ligand sites.

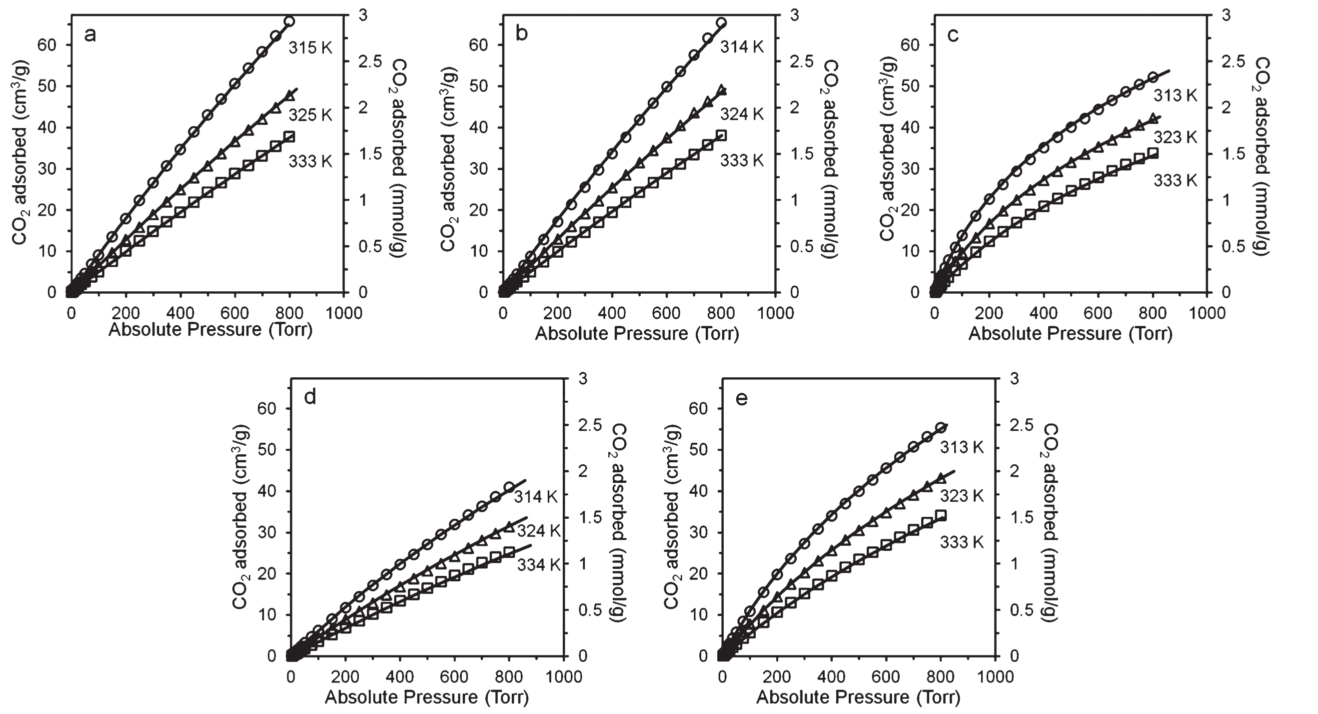

Fig. 6 Isotherms for the adsorption of CO_2 in (a) $Cu_3(BTC)_2$, (b) $Cr_3(BTC)_2$, $Ni_3(BTC)_2(DMF)_2(H_2O)$, (d) $Mo_3(BTC)_2(DMF)_{0.5}$, and (e) $[Ru_3(BTC)_2][BTC]_{0.5}$. Solid lines represent fits to the adsorption isotherms obtained using virial equations.

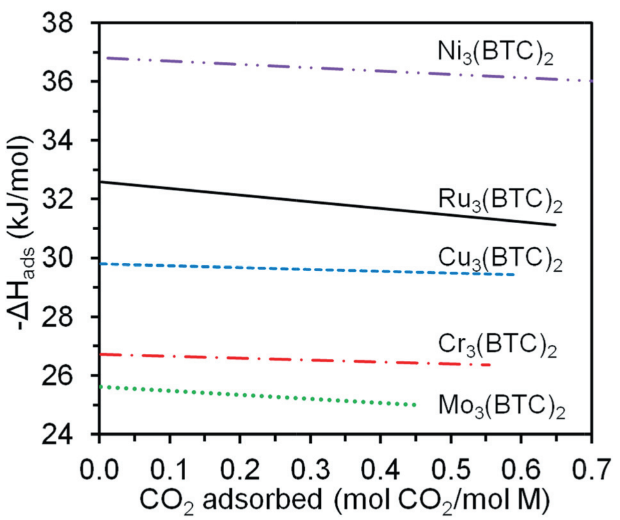

Fig. 7 Plot of isotherm-derived isosteric heats of adsorption *versus* CO_2 adsorbed per metal center for $M_3(BTC)_2(guest)_x$ (M = Cu, Cr, Mo, Ru).

The low CO_2 coverage in the measurements is reflected in a plot of the adsorption enthalpies *versus* CO_2 adsorbed (Fig. 7) which shows only slight decreases in the enthalpies from zero-coverage to the maximum CO_2 adsorbed. The zero-coverage isosteric heats of CO_2 adsorption measured for this series (25.6–32.6 kJ mol^{-1}) are in line with those observed for MOFs containing UMCs (21–47 kJ mol^{-1}), but considerably lower than values reported for amine functionalized materials (38–96 kJ mol^{-1}) measured using adsorption isotherms.[7] Moreover, the CO_2 adsorption enthalpy measured for $Cu_3(BTC)_2$ (29.8 kJ mol^{-1}) is close to the values obtained by Wang (−35 kJ mol^{-1})[24] and Xiang (−28.0 kJ mol^{-1}).[38] Both Cr_2BTC_3 and $Mo_3(BTC)_2(DMF)_{0.5}$ showed slightly lower zero coverage heats of CO_2 adsorption of 26.7 kJ mol^{-1} and 25.6 kJ mol^{-1}, respectively. Neutron scattering and spectroscopic studies of H_2 adsorption in $Cr_3(BTC)_2$ have suggested that the exposed Cr^{2+} sites are not occupied at low H_2 loading.[67] Indeed, the same scenario may hold for CO_2 adsorption by $Cr_3(BTC)_2$ and $Mo_3(BTC)_2(DMF)_{0.5}$ in this study. This would explain their similar enthalpies and lower affinity *versus* $Cu_3(BTC)_2$, where the Cu^{2+} center has been shown to be the initial site of interaction with CO_2 at low loading (1–1.5 CO_2–Cu).[42] In contrast, both $[Ru_3(BTC)_2][BTC]_{0.5}$ and $Ni_3(BTC)_2(Me_2NH)_2(H_2O)$ exhibited higher CO_2 adsorption enthalpies of 32.6 and 36.8 kJ mol^{-1}, respectively. In the case of the Ru analogue, this higher affinity may be assigned to the greater positive charge of the diruthenium units (5+) *versus* the other dimetal units (4+) in the series, but could also be due to CO_2 interaction with the Lewis basic, extra-framework BTC^{3-} anions. The higher CO_2 affinity exhibited by the $Ni_3(BTC)_2(Me_2NH)_2(H_2O)$ sample seemed surprising since few, if any, open Ni^{2+} centers should be exposed given the presence of coordinating guest molecules. However, experiments carried out by Snurr and coworkers have shown that slightly hydrated $Cu_3(BTC)_2$ exhibits increased and steeper CO_2 uptake *versus* fully evacuated samples.[59] This behavior agreed with grand canonical Monte Carlo simulations which indicated increased interaction energy due to Coulombic interactions between the coordinated water molecules and CO_2. In the present case, similar effects could be responsible for the higher heat of CO_2 adsorption displayed by $Ni_3(BTC)_2(Me_2NH)_2(H_2O)$, despite a diminished apparent surface area and overall CO_2 uptake due to guest molecules.

Conclusions

Increased BET surface areas (on a molar basis) have been obtained for the members of the $M_3(BTC)_2$ isostructural series M = Ni, Mo, Ru using improved activation procedures and syntheses. In the case of M = Mo, a solvent exchange procedure with methanol provided a material with only a small amount of residual DMF guest molecules. Likewise, methanol exchange carried out on a sample of $Ni_3(BTC)_2$ prior to evacuation resulted in an increased apparent BET surface area, but elemental analysis supported the presence of guest solvent molecules and an empirical formula of $Ni_3(BTC)_2(Me_2NH)_2(H_2O)$. An alternative procedure adopted for the synthesis of the Ru analog afforded a crystalline product formulated as $[Ru_3(BTC)_2]$-$[BTC]_{0.5}$. Despite the presence of BTC^{3-} guest anions in this structure, the material exhibited only a moderately decreased surface area *versus* the Cu, Cr, and Mo analogues. Samples of $Fe_3(BTC)_2Cl$ and $Zn_3(BTC)_2$ could be prepared according to literature procedures, but the resulting materials showed no indication of N_2 accessible microporosity.

Variable temperature CO_2 adsorption studies on the porous members of the $M_3(BTC)_2$ isostructural series revealed zero coverage isosteric heats of CO_2 adsorption consistent with those reported for MOFs containing UMCs. We found that in this series the heat of adsorption varied as Ni > Ru > Cu > Mo ≈ Cr. Due to the presence of donor guest molecules, it seems unlikely that the high enthalpy of adsorption observed for $Ni_3(BTC)_2$-$(Me_2NH)_2(H_2O)$ is due to metal–CO_2 interactions, and we speculate that the guests may play a role in the increased affinity. The differences observed among the remainder of the series support the notion that metal identity affects the strength of the initial framework–CO_2 interaction. Notably, $[Ru_3(BTC)_2]$-$[BTC]_{0.5}$, which bears a higher formal charge on the dimetal unit than the other isostructural MOFs, exhibited a slightly higher CO_2 adsorption enthalpy than the Cr, Cu, and Mo analogues. We attribute this behavior to the formation of stronger electrostatic interactions between CO_2 and the $\{Ru_2\}^{5+}$ sites. This interpretation is in agreement with the higher enthalpy reported for the more ionic $Mg_2(DOBDC)$ (39–47 kJ mol^{-1}) *versus* the isostructural and softer Co (37 kJ mol^{-1}) and Ni (37–42 kJ mol^{-1}) derivatives.[26,28,29,31] However, a potential interaction between CO_2 and the Lewis basic BTC^{3-} anions residing in the Ru material may contribute to the observed increase in adsorption enthalpy here. Overall, these results suggest that the use of more electropositive divalent metals, such as Mg^{2+}, or incorporation of more highly charged dimetal units could lead to $M_3(BTC)_2$ analogues with increased CO_2 affinity at low coverage.

Experimental

General considerations

Trimesic acid (Aldrich), $Cr(CO)_6$ (Strem), $Ni(NO_3)_2·6H_2O$ (Strem), $Cu(NO_3)_2·2.5H_2O$ (Strem), $Mo(CO)_6$ (Strem), $RuCl_3·xH_2O$ (Pressure Chemical), *N*,*N*-dimethylformamide (99.8%, VWR), and ethanol (ACS grade, Mallinckrodt) were used as received unless otherwise noted. $Fe_3(BTC)_2Cl$,[53] $Zn_3(BTC)_2$,[51] $Cu_3(BTC)_2$,[55] $Cr_3(BTC)_2$,[48] and $Ru_2(OPv)_4Cl$[68] were prepared according to literature procedures. Powder X-ray diffraction patterns were collected on a Bruker Advance D8 diffractometer using Nickel-filtered Cu-K_α radiation (λ = 1.5418 Å). Powder X-ray diffraction samples were prepared by placing a thin layer of sample on a glass slide inside a polyurethane domed sample holder. IR spectra were collected using either a Bruker Tensor 37 or Bruker Alpha (contained in a N_2-filled glovebox) FTIR spectrometer, both equipped with a diamond crystal Bruker Platinum ATR accessory. Raman spectra were collected using a Horiba Raman Microscope with a 633 nm laser. Thermogravimetric analysis (TGA) was performed on a TA Instruments Q500 Thermogravimetric Analyzer at a heating rate of 1 °C min^{-1} under a nitrogen gas flow of 90 mL min^{-1}. Elemental analyses were performed at Midwest Microlabs (Indianapolis, IN).

Gas sorption measurements

A Micromeritics ASAP 2020 Surface Area and Porosity Analyzer was used to measure N_2 and CO_2 adsorption isotherms. Oven-dried sample tubes equipped with TranSeals™ (Micrometrics) were evacuated and tared. Samples (100–200 mg) were transferred to the sample tube, which was then capped by a TranSeal™. Samples were heated to the appropriate temperatures and held at those temperatures until the outgas rate was less than 2 mTorr min^{-1}. The evacuated sample tubes were weighed again and the sample mass was determined by subtracting the mass of the previously tared tubes. N_2 adsorption isotherms were measured volumetrically at 77 K. Surface areas were calculated by fitting the isotherm data to the BET equation with the appropriate pressure range ($0.0001 \le P/P_0 \le 0.1$) determined by the consistency criteria of Rouquerol.[69,70] The reported errors in the BET surface area values are based on the fitting to the BET equation. CO_2 isotherms were measured between 313 and 334 K using a Micrometrics thermocouple-controlled heating mantle. Ultra high purity grade (99.999% purity) N_2, CO_2, and He, oil-free valves and gas regulators were used for all free space corrections and measurements. Isosteric heats of adsorption were calculated by fitting the adsorption isotherms to a virial equation.[66]

Synthesis of $[Mo_3(BTC)_2][DMF]_{0.5}$

A dry 100 mL Schlenk flask was charged with $Mo(CO)_6$ (1.13 g, 4.28 mmol), trimesic acid (0.75 g, 3.57 mmol), and degassed DMF (60 mL) under a nitrogen atmosphere. The reaction mixture was heated to reflux with rapid stirring for 1 week after which a fine orange–red solid separated. The flask was cooled to room temperature and the solids were separated by filtration and washed with dry, degassed DMF (3 × 20 mL). The product was soaked in methanol for 1 week at ambient temperature, and the solvent was refreshed daily to facilitate DMF exchange. After 1 week, the solid was filtered and dried *in vacuo* at room temperature to afford 0.38 g (36%) of light orange powder. The material was further activated by heating in vacuum at 100 °C for 12 h and at 150 °C for 24 h. Elemental analysis calcd for $Mo_3(C_9H_3O_6)_2(C_3H_7NO)_{0.5}$: C, 31.71; H, 1.30; N, 0.95. Found: C, 32.06; H, 1.47; N 1.05.

Synthesis of $[Ru_3(BTC)_2][BTC]_{0.5}$

A 23 mL Teflon-lined acid digestion bomb was charged with $Ru_2(OPv)_4Cl$ (0.54 g, 0.84 mmol), trimesic acid (0.24 g, 1.14 mmol), acetic acid (161 μL, 2.8 mmol), and H_2O (12 mL). The reaction vessel was sealed and heated in an oven to 160 °C for 4 days. After allowing to cool to room temperature, the product was collected by filtration as a dark brown powder, washed with ethanol (3 × 10 mL), and dried *in vacuo* at room temperature to afford 0.27 g (72%) of product. The sample was activated by heating under vacuum at 150 °C for 48 h. Elemental analysis calcd for $Ru_3(C_9H_3O_6)_2(C_9H_3O_6)_{0.5}$: C, 32.91; H, 0.92; Cl 0.0. Found: C, 32.79; H, 1.46; Cl, trace.

Synthesis of $Ni_3(BTC)_2(Me_2NH)_2(H_2O)$

This procedure could be carried out in either a 23 mL Teflon-lined acid digestion bomb or a 75 mL thick-walled glass bomb with a Teflon screw cap (Synthware). In a representative procedure, the glass reactor was charged with $Ni(NO_3)_2{\cdot}6H_2O$ (0.76 g, 2.6 mmol), trimesic acid (0.41 g, 1.9 mmol), 2-methylimidazole (0.11 g, 1.3 mmol), and dry, degassed DMF (30 mL). The vessel was sealed and heated in an oven to 170 °C for 2 days. After allowing to cool to room temperature, a mixture of the solvent and brown powder was decanted from the green crystals which had separated on the inside of the glass. The green crystals were then washed with DMF (5 × 10 mL) to remove any of the remaining powder and dried *in vacuo* at room temperature to afford 0.160 g (17%) of product. The product was soaked in methanol for 24 h at ambient temperature, and the solvent was refreshed once after 12 h. The resulting material was filtered, dried in vacuum for 12 h at room temperature, and further activated by heating under vacuum at 150 °C for 24 h. Elemental analysis calcd for $Ni_3(BTC)_2(Me_2NH)_2(H_2O)$: C, 37.83; H, 3.17; N, 4.01. Found: C, 37.96; H, 3.25; N 4.77.

Acknowledgements

This work was supported by the MIT Energy Initiative through a Seed Fund to MD. We thank Prof. Yang Shao-Horn for use of the Raman spectrometer.

Notes and references

1 J.-R. Li, R. J. Kuppler and H.-C. Zhou, *Chem. Soc. Rev.*, 2009, **38**, 1477–1504.
2 R. E. Morris and P. S. Wheatley, *Angew. Chem., Int. Ed.*, 2008, **47**, 4966–4981.
3 S. Kitagawa, R. Kitaura and S.-i. Noro, *Angew. Chem., Int. Ed.*, 2004, **43**, 2334–2375.
4 G. Ferey, *Chem. Soc. Rev.*, 2008, **37**, 191–214.
5 L. J. Murray, M. Dincă and J. R. Long, *Chem. Soc. Rev.*, 2009, **38**, 1294–1314.
6 R. J. Kuppler, D. J. Timmons, Q.-R. Fang, J.-R. Li, T. A. Makal, M. D. Young, D. Yuan, D. Zhao, W. Zhuang and H.-C. Zhou, *Coord. Chem. Rev.*, 2009, **253**, 3042–3066.
7 K. Sumida, D. L. Rogow, J. A. Mason, T. M. McDonald, E. D. Bloch, Z. R. Herm, T.-H. Bae and J. R. Long, *Chem. Rev.*, 2012, **112**, 724–781.
8 J. Liu, P. K. Thallapally, B. P. McGrail, D. R. Brown and J. Liu, *Chem. Soc. Rev.*, 2012, **41**, 2308–2322.
9 S. Keskin, T. M. van Heest and D. S. Sholl, *ChemSusChem*, 2010, **3**, 879–891.
10 G. Ferey, C. Serre, T. Devic, G. Maurin, H. Jobic, P. L. Llewellyn, G. De Weireld, A. Vimont, M. Daturi and J. S. Chang, *Chem. Soc. Rev.*, 2011, **40**, 550–562.
11 J. R. Li, Y. G. Ma, M. C. McCarthy, J. Sculley, J. M. Yu, H. K. Jeong, P. B. Balbuena and H. C. Zhou, *Coord. Chem. Rev.*, 2011, **255**, 1791–1823.
12 Q. Wang, J. Luo, Z. Zhong and A. Borgna, *Energy Environ. Sci.*, 2011, **4**, 42–55.
13 C. Janiak and J. K. Vieth, *New J. Chem.*, 2010, **34**, 2366–2388.
14 D. M. D'Alessandro, B. Smit and J. R. Long, *Angew. Chem., Int. Ed.*, 2010, **49**, 6058–6082.
15 A. R. Millward and O. M. Yaghi, *J. Am. Chem. Soc.*, 2005, **127**, 17998–17999.
16 B. Arstad, H. Fjellvaag, K. O. Kongshaug, O. Swang and R. Blom, *Adsorption*, 2008, **14**, 755–762.
17 S. Couck, J. F. M. Denayer, G. V. Baron, T. Remy, J. Gascon and F. Kapteijn, *J. Am. Chem. Soc.*, 2009, **131**, 6326–6327.
18 R. Vaidhyanathan, S. S. Iremonger, K. W. Dawson and G. K. H. Shimizu, *Chem. Commun.*, 2009, 5230–5232.
19 J. An, S. J. Geib and N. L. Rosi, *J. Am. Chem. Soc.*, 2010, **132**, 38–39.
20 T. M. McDonald, D. M. D'Alessandro, R. Krishna and J. R. Long, *Chem. Sci.*, 2011, **2**, 2022–2028.
21 E. Stavitski, E. A. Pidko, S. Couck, T. Remy, E. J. M. Hensen, B. M. Weckhuysen, J. Denayer, J. Gascon and F. Kapteijn, *Langmuir*, 2011, **27**, 3970–3976.
22 K. C. Stylianou, J. E. Warren, S. Y. Chong, J. Rabone, J. Bacsa, D. Bradshaw and M. J. Rosseinsky, *Chem. Commun.*, 2011, **47**, 3389–3391.
23 R. Vaidhyanathan, J. Liang, S. S. Iremonger and G. K. H. Shimizu, *Supramol. Chem.*, 2011, **23**, 278–282.
24 Q. M. Wang, D. M. Shen, M. Bulow, M. L. Lau, S. G. Deng, F. R. Fitch, N. O. Lemcoff and J. Semanscin, *Microporous Mesoporous Mater.*, 2002, **55**, 217–230.
25 A. Vimont, J. M. Goupil, J. C. Lavalley, M. Daturi, S. Surble, C. Serre, F. Millange, G. Ferey and N. Audebrand, *J. Am. Chem. Soc.*, 2006, **128**, 3218–3227.
26 P. D. C. Dietzel, V. Besikiotis and R. Blom, *J. Mater. Chem.*, 2009, **19**, 7362–7370.
27 P. L. Llewellyn, S. Bourrelly, C. Serre, A. Vimont, M. Daturi, L. Hamon, G. De Weireld, J. S. Chang, D. Y. Hong, Y. K. Hwang, S. H. Jhung and G. Ferey, *Langmuir*, 2008, **24**, 7245–7250.
28 S. R. Caskey, A. G. Wong-Foy and A. J. Matzger, *J. Am. Chem. Soc.*, 2008, **130**, 10870–10871.
29 P. D. C. Dietzel, R. E. Johnsen, H. Fjellvag, S. Bordiga, E. Groppo, S. Chavan and R. Blom, *Chem. Commun.*, 2008, 5125–5127.
30 A. O. Yazaydin, R. Q. Snurr, T. H. Park, K. Koh, J. Liu, M. D. LeVan, A. I. Benin, P. Jakubczak, M. Lanuza, D. B. Galloway, J. J. Low and R. R. Willis, *J. Am. Chem. Soc.*, 2009, **131**, 18198–18199.
31 D. Britt, H. Furukawa, B. Wang, T. G. Glover and O. M. Yaghi, *Proc. Natl. Acad. Sci. U. S. A.*, 2009, **106**, 20637–20640.
32 D. Farrusseng, C. Daniel, C. Gaudillere, U. Ravon, Y. Schuurman, C. Mirodatos, D. Dubbeldam, H. Frost and R. Q. Snurr, *Langmuir*, 2009, **25**, 7383–7388.
33 A. Demessence, D. M. D'Alessandro, M. L. Foo and J. R. Long, *J. Am. Chem. Soc.*, 2009, **131**, 8784–8786.
34 B. L. Chen, S. C. Xiang and G. D. Qian, *Acc. Chem. Res.*, 2010, **43**, 1115–1124.
35 K. Sumida, S. Horike, S. S. Kaye, Z. R. Herm, W. L. Queen, C. M. Brown, F. Grandjean, G. J. Long, A. Dailly and J. R. Long, *Chem. Sci.*, 2010, **1**, 184–191.
36 E. D. Bloch, D. Britt, C. Lee, C. J. Doonan, F. J. Uribe-Romo, H. Furukawa, J. R. Long and O. M. Yaghi, *J. Am. Chem. Soc.*, 2010, **132**, 14382–14384.
37 A. C. Kizzie, A. G. Wong-Foy and A. J. Matzger, *Langmuir*, 2011, **27**, 6368–6373.
38 Z. H. Xiang, Z. Hu, D. P. Cao, W. T. Yang, J. M. Lu, B. Y. Han and W. C. Wang, *Angew. Chem., Int. Ed.*, 2011, **50**, 491–494.
39 J. A. Mason, K. Sumida, Z. R. Herm, R. Krishna and J. R. Long, *Energy Environ. Sci.*, 2011, **4**, 3030–3040.
40 E. F. da Silva and H. F. Svendsen, *Int. J. Greenhouse Gas Control*, 2007, **1**, 151–157.
41 G. T. Rochelle, *Science*, 2009, **325**, 1652–1654.
42 H. Wu, J. M. Simmons, G. Srinivas, W. Zhou and T. Yildirim, *J. Phys. Chem. Lett.*, 2010, **1**, 1946–1951.
43 W. Zhou, H. Wu and T. Yildirim, *J. Am. Chem. Soc.*, 2008, **130**, 15268–15269.

44 S. S. Kaye and J. R. Long, *J. Am. Chem. Soc.*, 2005, **127**, 6506–6507.
45 M. Dincă and J. R. Long, *J. Am. Chem. Soc.*, 2007, **129**, 11172–11176.
46 W. L. Queen, C. M. Brown, D. K. Britt, P. Zajdel, M. R. Hudson and O. M. Yaghi, *J. Phys. Chem. C*, 2011, **115**, 24915–24919.
47 S. S. Y. Chui, S. M. F. Lo, J. P. H. Charmant, A. G. Orpen and I. D. Williams, *Science*, 1999, **283**, 1148–1150.
48 L. J. Murray, M. Dincă, J. Yano, S. Chavan, S. Bordiga, C. M. Brown and J. R. Long, *J. Am. Chem. Soc.*, 2010, **132**, 7856–7857.
49 M. Kramer, S. B. Ulrich and S. Kaskel, *J. Mater. Chem.*, 2006, **16**, 2245–2248.
50 Q. R. Fang, G. S. Zhu, M. H. Xin, D. L. Zhang, X. Shi, G. Wu, G. Tian, L. L. Tang, M. Xue and S. L. Qiu, *Chem. J. Chin. Univ.-Chin.*, 2004, **25**, 1016–1018.
51 J. I. Feldblyum, M. Liu, D. W. Gidley and A. J. Matzger, *J. Am. Chem. Soc.*, 2011, **133**, 18257–18263.
52 P. Maniam and N. Stock, *Inorg. Chem.*, 2011, **50**, 5085–5097.
53 L. Xie, S. Liu, C. Gao, R. Cao, J. Cao, C. Sun and Z. Su, *Inorg. Chem.*, 2007, **46**, 7782–7788.
54 O. Kozachuk, K. Yusenko, H. Noei, Y. M. Wang, S. Walleck, T. Glaser and R. A. Fischer, *Chem. Commun.*, 2011, **47**, 8509–8511.
55 J. Liu, Y. Wang, A. I. Benin, P. Jakubczak, R. R. Willis and M. D. LeVan, *Langmuir*, 2010, **26**, 14301–14307.
56 A. G. Wong-Foy, A. J. Matzger and O. M. Yaghi, *J. Am. Chem. Soc.*, 2006, **128**, 3494–3495.
57 J. Liu, J. T. Culp, S. Natesakhawat, B. C. Bockrath, B. Zande, S. G. Sankar, G. Garberoglio and J. K. Johnson, *J. Phys. Chem. C*, 2007, **111**, 9305–9313.
58 M. Hartmann, S. Kunz, D. Himsl, O. Tangermann, S. Ernst and A. Wagener, *Langmuir*, 2008, **24**, 8634–8642.
59 A. O. Yazaydin, A. I. Benin, S. A. Faheem, P. Jakubczak, J. J. Low, R. R. Willis and R. Q. Snurr, *Chem. Mater.*, 2009, **21**, 1425–1430.
60 T. Duren, F. Millange, G. Ferey, K. S. Walton and R. Q. Snurr, *J. Phys. Chem. C*, 2007, **111**, 15350–15356.
61 M. Dincă, A. Dailly, Y. Liu, C. M. Brown, D. A. Neumann and J. R. Long, *J. Am. Chem. Soc.*, 2006, **128**, 16876–16883.
62 H. A. Al-Abadleh and V. H. Grassian, *Langmuir*, 2003, **19**, 341–347.
63 I. A. Beta, H. Bohlig and B. Hunger, *Phys. Chem. Chem. Phys.*, 2004, **6**, 1975–1981.
64 S. Bordiga, L. Regli, C. Lamberti, A. Zecchina, M. Bjorgen and K. P. Lillerud, *J. Phys. Chem. B*, 2005, **109**, 7724–7732.
65 K. C. Szeto, C. Prestipino, C. Lamberti, A. Zecchina, S. Bordiga, M. Bjorgen, M. Tilset and K. P. Lillerud, *Chem. Mater.*, 2007, **19**, 211–220.
66 L. Czepirski and J. Jagiello, *Chem. Eng. Sci.*, 1989, **44**, 797–801.
67 K. Sumida, J. H. Her, M. Dincă, L. J. Murray, J. M. Schloss, C. J. Pierce, B. A. Thompson, S. A. FitzGerald, C. M. Brown and J. R. Long, *J. Phys. Chem. C*, 2011, **115**, 8414–8421.
68 M. C. Barral, R. Jimenezaparicio, J. L. Priego, E. C. Royer, M. J. Saucedo, F. A. Urbanos and U. Amador, *J. Chem. Soc., Dalton Trans.*, 1995, 2183–2187.
69 J. Rouquerol, P. Llewellyn and F. Rouquerol, *Stud. Surf. Sci. Catal.*, 2007, **160**, 49–56.
70 K. S. Walton and R. Q. Snurr, *J. Am. Chem. Soc.*, 2007, **129**, 8552–8556.